






Accelerated free-breathing whole-heart 3D T_2 mapping with high isotropic resolution

Aurélien Bustin¹   | Giorgia Milotta¹  | Tevfik F. Ismail¹ | Radhouene Neji^{1,2} | René M. Botnar^{1,3}  | Claudia Prieto^{1,3} 

¹Department of Biomedical Engineering, School of Biomedical Engineering and Imaging Sciences, King's College London, London, United Kingdom

²MR Research Collaborations, Siemens Healthcare, Frimley, United Kingdom

³Escuela de Ingeniería, Pontificia Universidad Católica de Chile, Santiago, Chile

Correspondence

Aurélien Bustin, School of Biomedical Engineering and Imaging Sciences, King's Health Partners, King's College London, 3rd Floor, Lambeth Wing, St. Thomas' Hospital, London SE1 7EH, United Kingdom.

Email: aurelien.bustin@kcl.ac.uk

Twitter: @AurelienBustin

Funding information

EPSRC (EP/P001009, EP/P032311/1, EPSRC EP/P007619), Wellcome EPSRC Centre for Medical Engineering (NS/A000049/1), and the Department of Health through the National Institute for Health Research Comprehensive Biomedical Research Centre Award to Guy's & St. Thomas' NHS Foundation Trust in partnership with King's College London and King's College Hospital NHS Foundation Trust.

Purpose: To enable free-breathing whole-heart 3D T_2 mapping with high isotropic resolution in a clinically feasible and predictable scan time. This 3D motion-corrected undersampled signal matched (MUST) T_2 map is achieved by combining an undersampled motion-compensated T_2 -prepared Cartesian acquisition with a high-order patch-based reconstruction.

Methods: The 3D MUST- T_2 mapping acquisition consists of an electrocardiogram-triggered, T_2 -prepared, balanced SSFP sequence with nonselective saturation pulses. Three undersampled T_2 -weighted volumes are acquired using a 3D Cartesian variable-density sampling with increasing T_2 preparation times. A 2D image-based navigator is used to correct for respiratory motion of the heart and allow 100% scan efficiency. Multicontrast high-dimensionality undersampled patch-based reconstruction is used in concert with dictionary matching to generate 3D T_2 maps. The proposed framework was evaluated in simulations, phantom experiments, and in vivo (10 healthy subjects, 2 patients) with 1.5-mm³ isotropic resolution. Three-dimensional MUST- T_2 was compared against standard multi-echo spin-echo sequence (phantom) and conventional breath-held single-shot 2D SSFP T_2 mapping (in vivo).

Results: Three-dimensional MUST- T_2 showed high accuracy in phantom experiments ($R^2 > 0.99$). The precision of T_2 values was similar for 3D MUST- T_2 and 2D balanced SSFP T_2 mapping in vivo (5 ± 1 ms versus 4 ± 2 ms, $P = .52$). Slightly longer T_2 values were observed with 3D MUST- T_2 in comparison to 2D balanced SSFP T_2 mapping (50.7 ± 2 ms versus 48.2 ± 1 ms, $P < .05$). Preliminary results in patients demonstrated T_2 values in agreement with literature values.

Conclusion: The proposed approach enables free-breathing whole-heart 3D T_2 mapping with high isotropic resolution in about 8 minutes, achieving accurate and precise T_2 quantification of myocardial tissue in a clinically feasible scan time.

KEYWORDSfast imaging, isotropic resolution, motion correction, myocardial T_2 mapping, T_2 quantification

1 | INTRODUCTION

Quantitative myocardial T_2 mapping has emerged as a promising tool for edema characterization and detection of subtle myocardial inflammation in patients with acute myocardial infarction, myocarditis, dilated cardiomyopathy, sarcoidosis, and autoimmune cardiomyopathies.¹⁻⁴

Myocardial T_2 mapping is usually performed by acquiring several electrocardiogram (ECG)-triggered T_2 -weighted images, with different amounts of T_2 decay through T_2 -preparation pulses. A map of T_2 relaxation times is then generated by fitting the series of weighted images to an exponential decay model on a pixel-by-pixel basis. Current clinical protocols usually perform myocardial T_2 mapping with a 2D single-shot SSFP (T_2 p-SSFP), acquiring 3 T_2 -prepared images in a single breath-hold every 2 to 3 heartbeats to allow for full T_1 recovery.³ Multiple short-axis slices are usually acquired at the basal, midventricular, and apical level.

However, the use of 2D acquisitions with fairly thick slices and the associated partial volume effects undermine the full potential of myocardial T_2 mapping, particularly in hypertrophic cardiomyopathies in which the pathological tissues are often complex 3D structures with differing T_2 values.⁵⁻⁷ Furthermore, 2D sequences, typically acquired during breath-holding, regularly suffer from respiratory and cardiac motion between the T_2 -weighted images, due primarily to imperfect breath-holding or variable heart rate.⁸ Although robust nonrigid motion-correction techniques have been proposed to correct for residual motion and improve map quality, such techniques are relatively complex, computationally expensive, and only correct for in-plane motion.⁹⁻¹¹

A free-breathing 3D T_2 mapping approach with high isotropic spatial resolution may have the potential to increase diagnostic accuracy in patients with acute myocardial injury (e.g., NSTEMI patients^{12,13}) and improve the detection of cardiac involvement in patients with systemic sarcoidosis.¹⁴

Three-dimensional myocardial T_2 mapping techniques have been proposed to address the limitations of 2D imaging by allowing for large coverage of the heart with inherently higher SNR. Non-Cartesian self-navigated myocardial T_2 mapping has been proposed to perform free-breathing 3D myocardial T_2 mapping at 3 T in about 18-minute acquisition time.^{5,15} Such long scan times, unfortunately, may impede the clinical integration of this technique. A self-navigated hybrid radial Cartesian trajectory was also proposed to perform free-breathing 3D myocardial T_2 mapping in less than 5 minutes, although with low spatial resolution.¹⁶ The use of saturation pulses at every heartbeat was proposed

to accelerate Cartesian 3D T_2 mapping.¹⁷ Long resting periods (in the order of 2-3 heartbeats^{3,5}) are usually needed in T_2 mapping to ensure full recovery of the longitudinal magnetization between acquisitions to minimize T_1 effects and satisfy the assumption that the equilibrium state magnetization is not affected by heart-rate variations throughout the scan. Nonselective 90° saturation pulses reset magnetization history by tipping the longitudinal magnetization of the imaged volume into the transverse plane, thus removing heart-rate dependency during the acquisition and allowing for imaging every heartbeat. This approach also eliminates artifacts caused by heart-rate variations, at the cost of a reduced SNR and lower precision of T_2 values. However, this technique uses prospective diaphragmatic navigator-gated acquisitions, thus leading to prolonged and often unpredictable scan times (about 9-minute nominal scan time with 30% to 60% respiratory gating efficiency), as only a small fraction of the acquired data is accepted for reconstruction (referred to as low scan efficiency).

Notwithstanding the continued advancements, myocardial 3D T_2 mapping still faces substantial technical challenges that in turn may limit its applicability in clinical practice. In this study, we sought to achieve high isotropic spatial resolution 3D Cartesian whole-heart myocardial T_2 mapping in a short and predictable scan time of about 8 minutes by combining a highly accelerated saturation-based free-breathing myocardial T_2 mapping sequence with 2D image-based navigator (iNAV) respiratory motion correction. A recently proposed high-dimensionality undersampled patch-based reconstruction (HD-PROST)¹⁸ is used in concert with dictionary matching, based on the extended phase graph formalism,¹⁹ to allow for accurate and precise myocardial T_2 maps. The proposed framework was validated in simulations, phantom, and healthy subject experiments, while its initial clinical feasibility was shown for 2 patients with suspected cardiovascular disease.

2 | METHODS

Acquisitions were performed on a 1.5T MR scanner (Magnetom Aera, Siemens Healthcare, Erlangen, Germany) with a dedicated 18-channel body coil and a 32-channel spine coil. Written informed consent was obtained from all healthy subjects and patients before undergoing MRI scans, and the study was approved by the National Research Ethics Service. Numerical simulations, reconstructions and analysis were performed on

a workstation with a 16-core dual Intel Xeon Processor (2.3 GHz, 256 GB RAM).

2.1 | Accelerated whole-heart 3D T₂ mapping sequence

The proposed myocardial 3D motion-corrected undersampled signal-matched (MUST) T₂ mapping sequence is shown in Figure 1. A saturation pulse is performed right after the R-wave with a constant saturation time (T_{SAT}) from the data acquisition. The value of T_{SAT} is set to the maximal available time allowed by the sequence to guarantee enough magnetization recovery before the next acquisition. This approach allows efficient imaging at every heartbeat, avoiding the use of multiple recovery periods.¹⁷ Subsequently, an adiabatic T₂ prepared pulse with variable TE (TE_{T₂prep}) is performed, followed by a balanced SSFP readout. An adiabatic T₂-prep module (Silver-Hoult type) is used because of its good insensitivity to B₁ and B₀ inhomogeneities.²⁰ Three T₂-weighted volumes are acquired sequentially with different T₂ weightings (TE_{T₂prep} = [0, 28, 55] ms).

A 3D Cartesian variable-density trajectory with spiral profile order^{21,22} is used to allow for fast acquisition of the 3 T₂-prepared volumes. This trajectory samples the k_y-k_z

phase-encoding plane following approximate spiral interleaves on the Cartesian grid with variable density along each spiral arm and with 2 successive spiral interleaves being rotated by the golden angle. A golden angle rotation^{21,23} between different contrast acquisitions was incorporated to introduce incoherently distributed aliasing along the contrast dimension and noise-like artifacts in the spatial dimension (Supporting Information Figure S1).

A 2D low-resolution iNAV²⁴ precedes the 3D acquisition at every heartbeat to enable 2D translational respiratory motion estimation/compensation (superior–inferior and right–left directions). This technique, already validated for coronary MRA²⁴ and multicontrast cardiac MRI,²⁵ enables 100% scan efficiency with predictable scan time, resulting in about 2-3 times acceleration compared with diaphragmatic navigator gate-based acquisitions. Two-dimensional iNAVs are obtained by spatially encoding the startup echoes of the balanced SSFP T₂-mapping sequence. Two-dimensional translational motion is estimated using a template-matching algorithm with normalized cross correlation as similarity measure, with the template manually selected around the heart during acquisition planning. Motion compensation of the 3 volumes is performed by modulating the k-space data with a linear phase shift to a reference respiratory position selected at end-expiration.²⁴

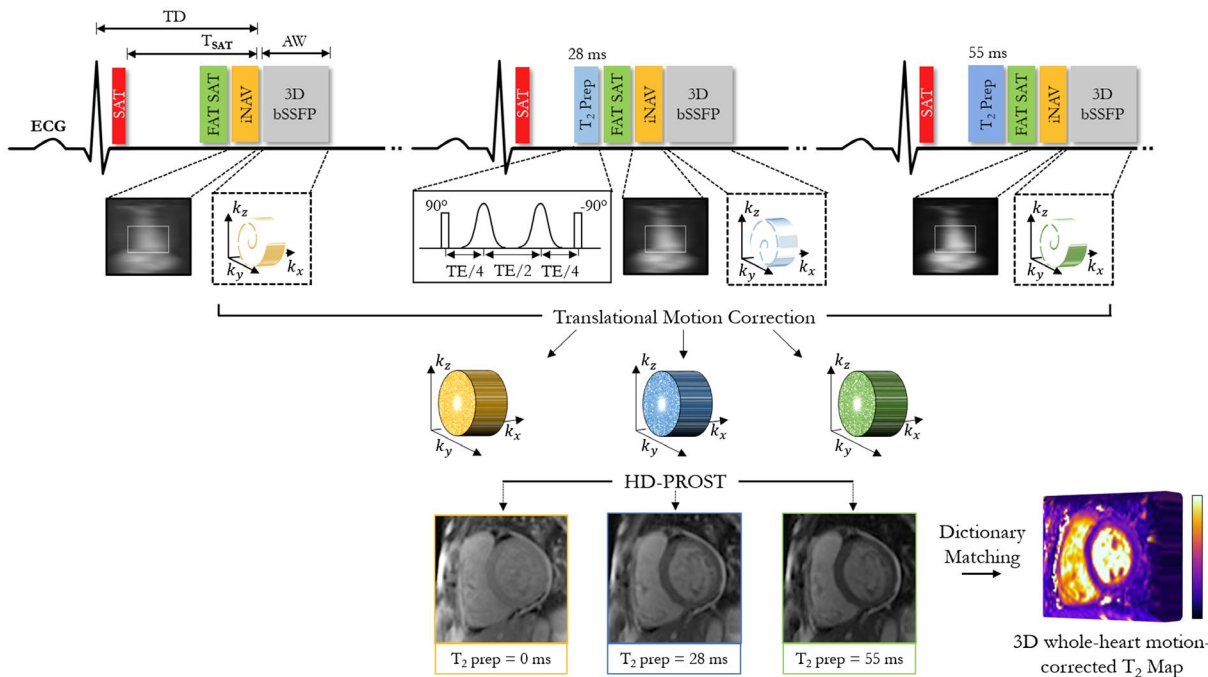


FIGURE 1 Schematic overview of the proposed free-breathing 3D motion-corrected undersampled signal matched (MUST) T₂ technique for whole-heart myocardial T₂ mapping. Three T₂-prepared volumes are acquired sequentially with increasing TE_{T₂prep} ([0,28,55] ms). A nonselective saturation pulse is applied immediately after the electrocardiogram (ECG) R-wave to avoid recovery heartbeats. A 2D image navigator is acquired to enable translational respiratory motion correction of the heart and shorter and predictable scan times. A golden-angle shifted variable-density Cartesian undersampling is used to achieve clinically feasible scan times. All T₂ prepared volumes are reconstructed simultaneously with high-dimensionality undersampled patch-based reconstruction (HD-PROST).¹⁸ A dictionary is then simulated and matched to the measured signal to generate the whole-heart T₂ maps. Abbreviations: AW, acquisition window; bSSFP, balanced SSFP; iNAV, image-based navigator; TD, trigger delay; T_{SAT}, saturation time

2.2 | Multicontrast HD-PROST reconstruction

Multicontrast HD-PROST^{18,22} is used to reconstruct the 3 undersampled T_2 -weighted volumes. The HD-PROST reconstruction exploits local (i.e., within a patch), nonlocal (i.e., between similar patches within a neighborhood), and contrast (i.e., between T_2 -weighted images) redundancies of the 3D volumes in an efficient low-rank formulation. The reconstruction is formulated as an iterative 2-step process: (1) an L2-norm regularized parallel-imaging reconstruction using the denoised multicontrast data from step 2 as a prior (optimization 1); and (2) an efficient high-order low-rank patch-based denoising (optimization 2, Supporting Information Figure S2). The first step is optimized by gradient descent, whereas the second step is optimized through high-order low-rank tensor decomposition. The performance of HD-PROST reconstruction relies primarily on 2 parameters that need to be carefully tuned to get the best reconstruction quality: (1) the patch size ($N = 5 \times 5 \times 5$ pixels in this study), reflecting the degree of structural information within each patch, and (2) the high-order singular value truncation parameter ($\lambda_p = 0.1$ in this study) that controls the amount of regularization.

The HD-PROST reconstruction was implemented and performed offline using the algorithm described in Bustin et al.¹⁸ Reconstruction parameters were optimized empirically (as previously reported) and are illustrated in Supporting Information Figure S2. We refer the reader to Bustin et al.^{18,26} for a detailed description of HD-PROST and the associated reconstruction parameters.

2.3 | Numerical simulations

Usually in myocardial T_2 mapping, the acquisition of each T_2 -weighted image is followed by a resting period of about 2-3 heartbeats to allow for full longitudinal magnetization relaxation. Numerical extended phase graph simulations were first performed to investigate the impact of removing recovery heartbeats and integrating saturation pulses on the longitudinal magnetization of 3D MUST- T_2 for tissues with different relaxation times T_1 . Simulations were performed for a T_2 of 50 ms and varying T_1 values (ranging from 700 ms to 1200 ms) with and without saturation pulses. Other relevant parameters used in the simulations were $TE_{T_2\text{prep}} = 55$ ms, $TR = 3.2$ ms, trigger delay = 856 ms, data-acquisition window of 100 ms, and a simulated heart rate of 60 beats per minute (bpm).

2.4 | Dictionary generation and matching

Three-dimensional MUST- T_2 dictionaries are simulated using the extended phase graph formalism^{19,27,28} for a range

of T_2 values. For both phantom and in vivo experiments, the dictionaries are calculated matching the subject-specific acquisition parameters with T_2 s in the range [minimum : step size : maximum] of [4:2:100, 105:5:200, 210:10:450] ms. Simulations show that the proposed method is not dependent on the used T_1 value (in the range of interest) for dictionary generation (Supporting Information Figure S3, where the simulation results are shown for different T_1 values ranging from 850 ms to 1200 ms with a step size of 50 ms); thus, T_1 is kept constant at 1100 ms for the phantom and in vivo experiments. The T_2 maps are obtained by voxel-wise matching of the measured and normalized signal to the closest (minimum least squares) extended phase graph-based dictionary entry. The choice of dictionary-based matching versus conventional mono-exponential curve fitting is justified in Supporting Information Figure S4.

2.5 | Phantom experiments

The proposed ECG-triggered 3D MUST- T_2 mapping sequence was evaluated in a standardized (TIMES) T_1/T_2 phantom containing 9 agarose-based tubes with relevant cardiac T_1 and T_2 combinations (range, T_1 : 255-1489 ms, T_2 : 44-243 ms).²⁹ Scan parameters for 3D MUST- T_2 included $TR = 3.13$ ms, $TE = 1.37$ ms, flip angle = 90° , $FOV = 187 \times 187 \times 156$ mm³, 1.5 mm³ isotropic resolution, bandwidth = 908 Hz/pixel, data-acquisition window = 100 ms, and $TE_{T_2\text{prep}} = [0, 28, 55]$ ms. Reference T_2 relaxation times for each vial were obtained using a multi-echo spin-echo (SE) sequence with 8 TEs ranging from 10 ms to 640 ms. In addition, conventional ECG-triggered 2D T_2 p-SSFP was performed for comparison purposes with the following imaging parameters: 1.9×1.9 mm² in-plane resolution, slice thickness = 8 mm, $TR/TE = 3.11/1.38$ ms, linear k-space reordering, bandwidth = 1184 Hz/pixel, $TE_{T_2\text{prep}} = [0, 25, 55]$ ms, flip angle = 70° , 3 recovery beats, and GRAPPA factor 2 with 36 k-space autocalibration lines. The T_2 relaxation times were obtained by mono-exponential curve fitting for both the SE and T_2 p-SSFP sequences.

2.5.1 | Impact of heart rate on T_2 accuracy

The impact of heart-rate differences on T_2 accuracy was assessed by performing multiple 3D MUST- T_2 phantom acquisitions with different simulated heart rates (ranging from 50 bpm to 100 bpm, step size 10 bpm). The trigger delay was set to 70% of the R-R interval and ranged from 420 ms to 840 ms, while the saturation time T_{SAT} was always set to the maximum allowed time (ranging from 370 ms to 790 ms). The acquisitions were performed fully sampled using the previously described variable-density trajectory with spiral profile order sampling.

2.5.2 | Impact of acceleration on T_2 accuracy

To study the impact of accelerating 3D MUST- T_2 on the accuracy of the T_2 values, several phantom acquisitions were performed with different undersampling factors ranging from 1-fold to 5-fold (step size 1). Additional acquisition parameters included simulated heart rate of 60 bpm, trigger delay of 680 ms, and saturation time $T_{SAT} = 630$ ms.

2.5.3 | Data analysis

Circular regions of interest were drawn on each vial for 3D MUST- T_2 , SE, and 2D T_2 p-SSFP sequences. For each vial, the average T_2 value was measured, and agreement among SE, 2D T_2 p-SSFP T_2 values, and the proposed approach was assessed using linear regression.

2.6 | In vivo experiments

2.6.1 | Healthy subjects

Ten healthy subjects (5 men and 5 women, mean age of 30 years [range: 26-36 years]) with no history of cardiovascular disease underwent ECG-triggered free-breathing 3D whole-heart T_2 mapping using the proposed 3D MUST- T_2 acquisition approach. Relevant scan parameters included FOV = $320 \times 320 \times 84$ -108 mm³, slice oversampling = 22%, 1.5-mm³ isotropic resolution, flip angle = 90°, $TE_{T_2\text{prep}} = [0, 28, 55]$ ms, subject-dependent middiastolic trigger delay (mean: 672 ms [range: 521-952 ms]), acquisition window (mean: 97 ms [range: 80-108 ms]), T_{SAT} (range: 470-900 ms), acceleration factor of $\times 5$, 14 linear ramp-up pulses for iNAV, and Hanning-filtered sinc pulse with a duration of 1 ms and time-bandwidth product of 4.5. To ensure adequate fat suppression, a spectral presaturation with inversion recovery was applied before imaging. All 3D MUST- T_2 mapping acquisitions were performed in the coronal plane.

Conventional 2D T_2 p-SSFP T_2 mapping³ was acquired for each subject for comparison purposes. Acquisition parameters were the same as for the phantom experiments. Three short-axis slices (basal, midcavity, apical) were acquired in 3 separate breath-holds of about 10 seconds each. A nonrigid motion correction was carried out inline to compensate for in-plane motion between the three 2D T_2 -weighted images.¹¹ Subsequently, T_2 maps were obtained by mono-exponential curve fitting.

2.6.2 | Patients

The feasibility and preliminary clinical performance of the proposed 3D MUST- T_2 sequence was assessed in 2 patients (2 men, ages 42 and 50 years) with suspected cardiovascular

disease. The same acquisition and reconstruction parameters as in the healthy subject study were used. The patient-specific saturation times were $T_{SAT} = 525$ ms (patient 1, average heart rate = 75 bpm, acquisition window = 98 ms) and $T_{SAT} = 595$ ms (patient 2, average heart rate = 65 bpm, acquisition window = 100 ms). Conventional 2D T_2 p-SSFP T_2 mapping was acquired for each patient with the same parameters as in the healthy subject study.

2.6.3 | Data analysis

The 3D MUST- T_2 maps were reformatted in the short-axis view to match the 2D T_2 p-SSFP slices. Regional differences in left ventricular T_2 relaxation times were assessed according to the 16-segment model of the American Heart Association.³⁰ The T_2 measurements were reported as mean \pm SD and assessed using the Student's t-test. Statistical differences in regional T_2 values among reformatted basal, midventricular, and apical short-axis slices were analyzed using repeated-measures 1-way analysis of variance with Bonferroni post hoc comparisons. All statistical analyses were performed using MATLAB (version 7.1, MathWorks, Natick, MA), and statistical significances were defined as a p -value $< .05$.

3 | RESULTS

3.1 | Numerical simulations

The impact of recovery times on the signal intensity (longitudinal magnetization) is depicted in Figure 2A,B for multiple T_1 relaxation times (ranging from 700 ms to 1200 ms). Although a clear dependency was observed when no saturation pulse was applied, necessitating about 2-3 resting periods to recover 96% of the signal intensity (Figure 2A), applying a "reset" saturation pulse¹⁷ at every heartbeat avoids recovery periods, at the cost of a lower signal intensity (Figure 2B).

3.2 | Phantom experiments

The average T_2 values obtained in the phantom experiments when increasing the simulated heart rate (from 50 bpm to 100 bpm) are depicted in Figure 2C. The T_2 relaxation times measured with the proposed 3D MUST- T_2 sequence showed no to little sensitivity to change of heart rate for all vials in comparison to SE reference measurements.

The accuracy of the T_2 values obtained with the proposed 3D MUST- T_2 approach in phantom is shown in Figure 3 for different acceleration factors. Excellent linear correlation was found between 3D MUST- T_2 and the ground-truth T_2 values obtained with SE, with high coefficients of determination ($R^2 > 0.99$) for all acceleration factors ($\times 1$ to $\times 5$), suggesting high accuracy of the proposed 3D sequence

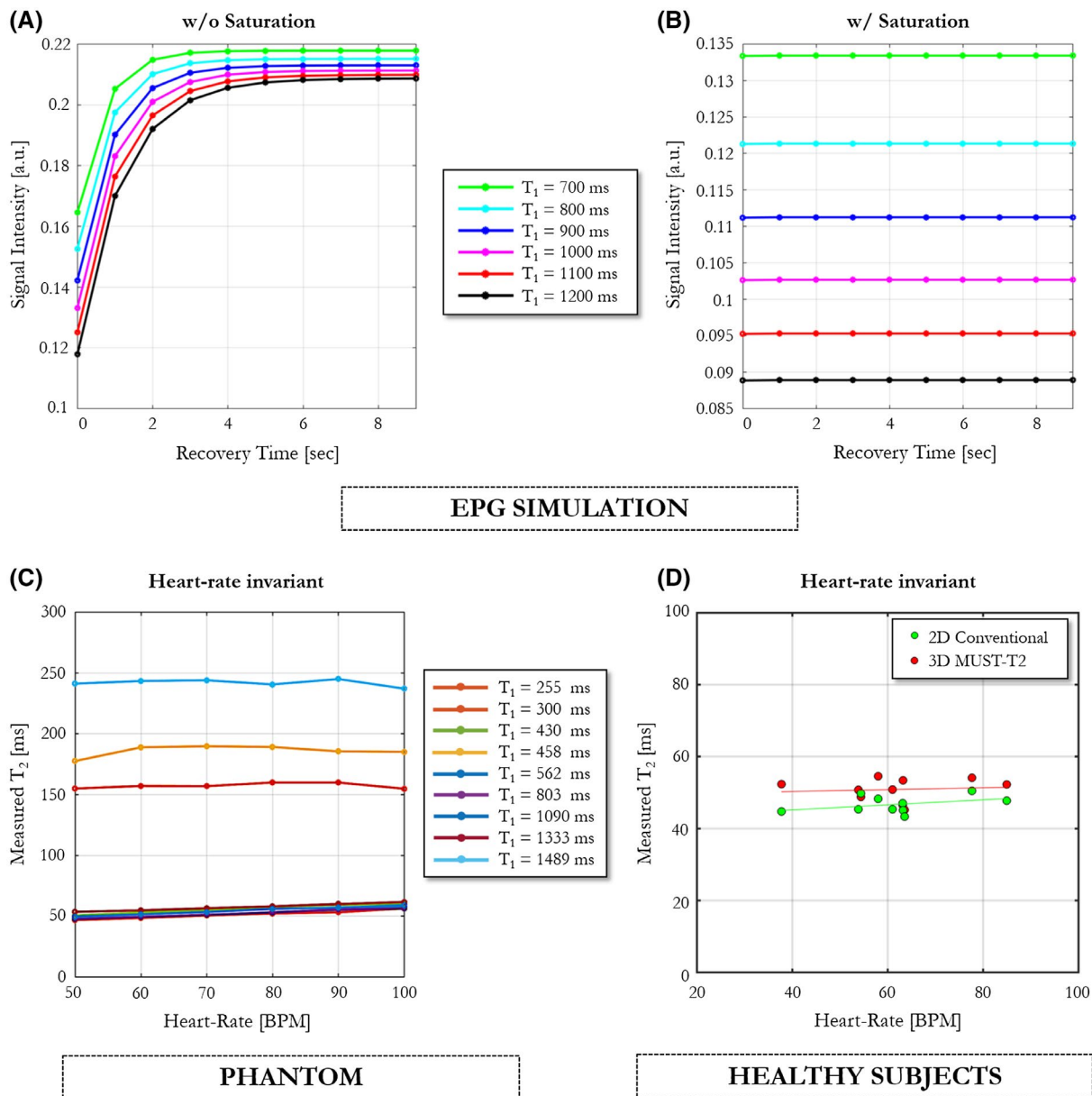


FIGURE 2 Results from extended phase graph (EPG) simulations show the effect of the saturation pulse on the MR signal evolution. A, Simulated magnetization obtained with the EPG formalism for different recovery times (ranging from 0 to 9 seconds) when the saturation pulse is not used. The signals were generated for tissues with a T_2 of 50 ms, varying T_1 s (ranging from 700 ms to 1200 ms), $TE_{T_2\text{prep}} = 50$ ms, and a simulated heart rate of 60 bpm. For long T_1 s, a minimum of about 6 idle heartbeats are needed to allow for full recovery of the longitudinal magnetization. B, When the saturation pulse is applied at every heartbeat, idle heartbeats are not required for signal recovery, at the cost of lower signal intensity. C, Evolution of the matched T_2 values obtained with the proposed 3D MUST- T_2 mapping sequence over different simulated heart rates (ranging from 50 bpm to 100 bpm) for each phantom vial. The proposed approach is mostly insensitive to heart-rate variations, even for long T_1 s. D, Effect of different heart rates across all healthy subjects ($N = 10$) on mean T_2 values. Abbreviations: BPM, beats per minute

even for high acceleration factors. Lower linear correlation ($R^2 = 0.95$) was observed for conventional 2D T_2 p-SSFP in comparison to reference SE measurements. Bias between SE and 2D T_2 p-SSFP with linear order acquisitions has been reported previously.³

Bland-Altman analysis demonstrated good T_2 agreement for all 31 slices of 3D MUST- T_2 (Supporting

Information Figure S5). The mean differences with 95% confidence interval (CI) between 3D MUST- T_2 and SE were 0.6 ms (95% CI, -2.1 ms to 0.89 ms) for short T_1 myocardium ($[T_2, T_1] = [48, 803]$ ms), 0.6 ms (95% CI, -3.7 to 2.5 ms) for medium T_1 myocardium ($[T_2, T_1] = [48, 1090]$ ms), and 1.4 ms (95% CI, -4.9 ms to -2.0 ms) for long T_1 myocardium ($[T_2, T_1] = [50, 1333]$ ms).

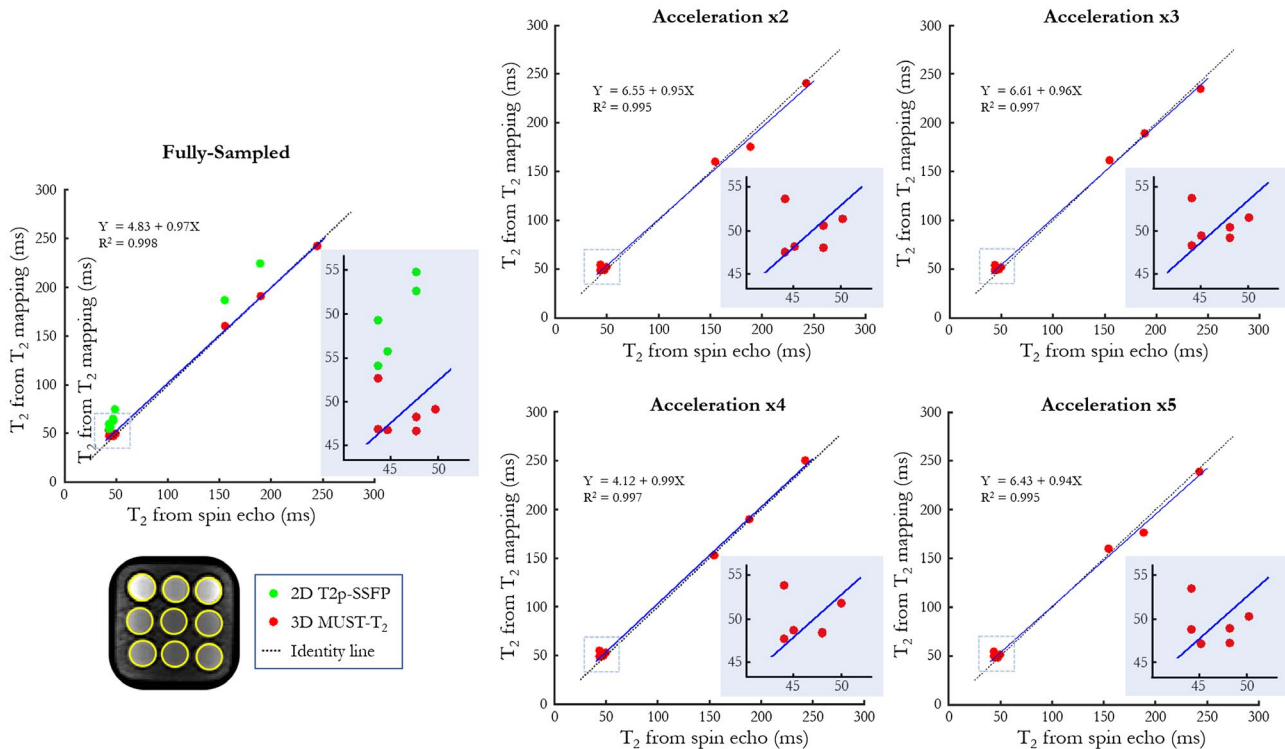


FIGURE 3 Phantom accuracy for the proposed 3D MUST- T_2 sequence. Plots compare the mean T_2 values derived from the 9 vials for 5 different acceleration factors with the ground-truth T_2 values (measured by spin echo [SE] with 8 TEs from 10–640 ms²⁹), conventional 2D T_2p -SSFP mapping (green), and the proposed 3D MUST- T_2 sequence. The T_2 accuracy is preserved with the proposed approach with excellent agreement with the reference T_2 values, even for high acceleration ($\times 5$). The T_2 values for the last tube ($T_2 = 250$ ms) were out of range (> 300 ms) for the 2D T_2p -SSFP sequence and therefore are not shown

3.3 | In vivo experiments

All healthy subject and patient acquisitions/reconstructions were performed successfully, and analysis results are reported hereafter.

3.3.1 | Healthy subjects

The average acquisition time of the proposed free-breathing 3D MUST- T_2 sequence in healthy subjects was 6 minutes 43seconds \pm 1 minute 37 seconds (range 4–10 minutes, heart rate range: 38–85 bpm) with 100% scan efficiency. Translational motion estimation and correction was performed in about 20 seconds, whereas the average reconstruction time (including HD-PROST reconstruction and dictionary matching) was about 3 minutes. Representative T_2 maps from 3 healthy subjects acquired with the proposed 3D MUST- T_2 sequence and the conventional 2D T_2p -SSFP sequence are shown in Figure 4. Both free-breathing 3D MUST- T_2 and breath-held 2D T_2p -SSFP show comparable visualization of the left ventricle and surrounding structures (e.g., papillary muscles). Reconstructed T_2 maps from additional healthy subjects are shown in Supporting Information Figure S6 and Supporting Information Figure S7.

Bull's eye plots based on the American Heart Association's 16-segment model of the left ventricle obtained with 3D MUST- T_2 and 2D T_2p -SSFP mappings are depicted in Figure 5A. A small, although significant, overestimation of regional T_2 values over the whole myocardium was observed with 3D MUST- T_2 in comparison to 2D T_2p -SSFP mapping (50.7 ± 1.7 ms for 3D MUST- T_2 versus 48.2 ± 1.3 ms for 2D T_2p -SSFP, $P < .05$). We found no statistical differences in regional T_2 values between segments with 3D MUST- T_2 for all subjects ($P = .6$). A small overestimation of septal T_2 values was observed with 3D MUST- T_2 in comparison to 2D T_2p -SSFP mapping with linear k-space reordering (mean difference: -4.2 ms, $\pm 95\%$ confidence interval: $-10.4/2.0$ ms, Figure 5B). Precision of T_2 values was similar for both techniques (5 ± 1 ms for 3D MUST- T_2 versus 4 ± 2 ms for 2D T_2p -SSFP, $P = .520$, Figure 5C). The corresponding average coefficient of variation for the proposed 3D MUST- T_2 approach was similar to that of the 2D conventional sequence (9.13% versus 9.09%, respectively, $P = .097$). There were no statistical differences in mean T_2 values with 3D MUST- T_2 among basal, midventricular, and apical slices for all subjects ($P = .655$).

The effect of heart-rate differences across healthy subjects on T_2 values is shown in Figure 2D. The T_2 measurements

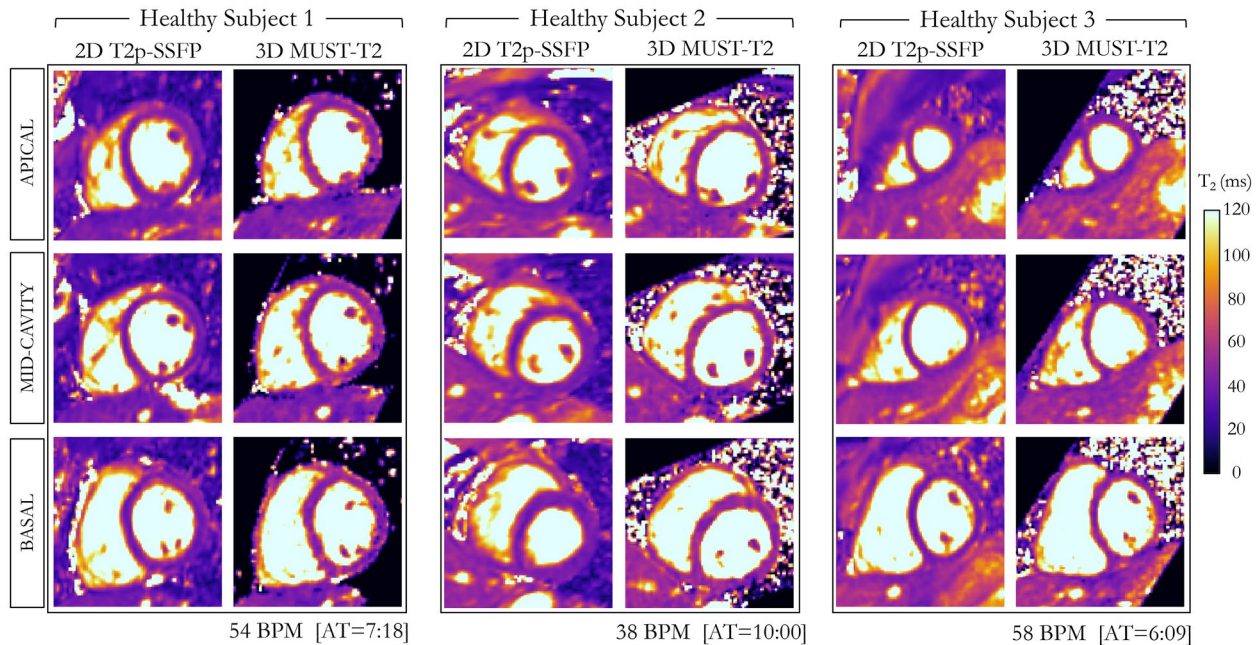


FIGURE 4 The T_2 maps obtained using the proposed free-breathing 3D MUST- T_2 sequence and the conventional breath-held 2D T_2 p-SSFP sequence are shown for 3 healthy subjects. The 3D MUST- T_2 slices were reformatted to short axis to match the 2D T_2 map acquisitions. Good visualization of the myocardium and surrounding structures can be observed on the 3D MUST- T_2 maps. Acquisition times are expressed as minutes:seconds. Abbreviations: AT, acquisition time

obtained from 3D MUST- T_2 in vivo showed no significant correlation with heart rate ($T_2 = 0.026 \times \text{heart rate} + 49$ ms, $P = .919$).

Eight short-axis slices of the left ventricular myocardium for 1 representative healthy subject obtained with the proposed 3D MUST- T_2 approach are shown in Figure 6. The reconstructed T_2 -weighted images and the corresponding T_2 maps are included. No noticeable residual undersampling artifacts were observed on the native T_2 -weighted images and corresponding T_2 maps for the entire left ventricle.

Because MUST- T_2 acquisitions were performed with isotropic spatial resolution and whole-heart coverage, the T_2 maps can be reformatted in any arbitrary plane. This advantage is best appreciated in Figure 7, where reformats in multiple standard orientations (short-axis, vertical long-axis, 3-chamber, and 4-chamber) are shown for a healthy subject.

The need for using 2D iNAV to correct for respiratory motion is shown in Supporting Information Figure S8, where the T_2 maps of 2 healthy subjects are shown with and without 2D translational motion correction. Motion-corrected T_2 maps result in better visualization of the myocardium as compared with the non-motion-corrected T_2 maps, which show some spatial blurring.

3.3.2 | Patients

No cardiac findings were observed in the patient study. The acquisition times of the proposed 3D MUST- T_2 sequence

were 7 minutes 23 seconds (patient 1, mean heart rate: 75 bpm) and 8 minutes 43 seconds (patient 2, mean heart rate: 65 bpm). Figure 8 depicts the reconstructed apical, midcavity, and basal T_2 map slices for the 2 patients, using the proposed 3D MUST- T_2 framework compared with the current clinical reference maps (breath-held 2D T_2 p-SSFP). The proposed 3D MUST- T_2 produces T_2 maps with visual appearance comparable to the conventional 2D T_2 p-SSFP technique. The mean septal T_2 relaxation times were similar between the 2 techniques (midventricular slice: patient 1: 48.2 ± 4 ms 3D MUST- T_2 versus 46.3 ± 3 ms 2D T_2 p-SSFP, and patient 2: 51.7 ± 7 ms 3D MUST- T_2 versus 50.8 ± 4 ms 2D T_2 p-SSFP).

4 | DISCUSSION

In this study, we proposed a framework for highly accelerated free-breathing whole-heart T_2 mapping that combines 2D translational respiratory motion correction with a golden-angle variable-density spiral-like Cartesian trajectory and a recently introduced HD-PROST reconstruction. The proposed 3D MUST- T_2 approach enables accurate and precise high-resolution isotropic (1.5 mm^3) 3D whole-heart T_2 mapping acquisitions in a fast and predictable scan time.

The performance of the proposed 3D T_2 mapping framework was assessed in simulations, phantom experiments, and 10 healthy subjects, while initial clinical feasibility was demonstrated in 2 patients with suspected cardiovascular disease.

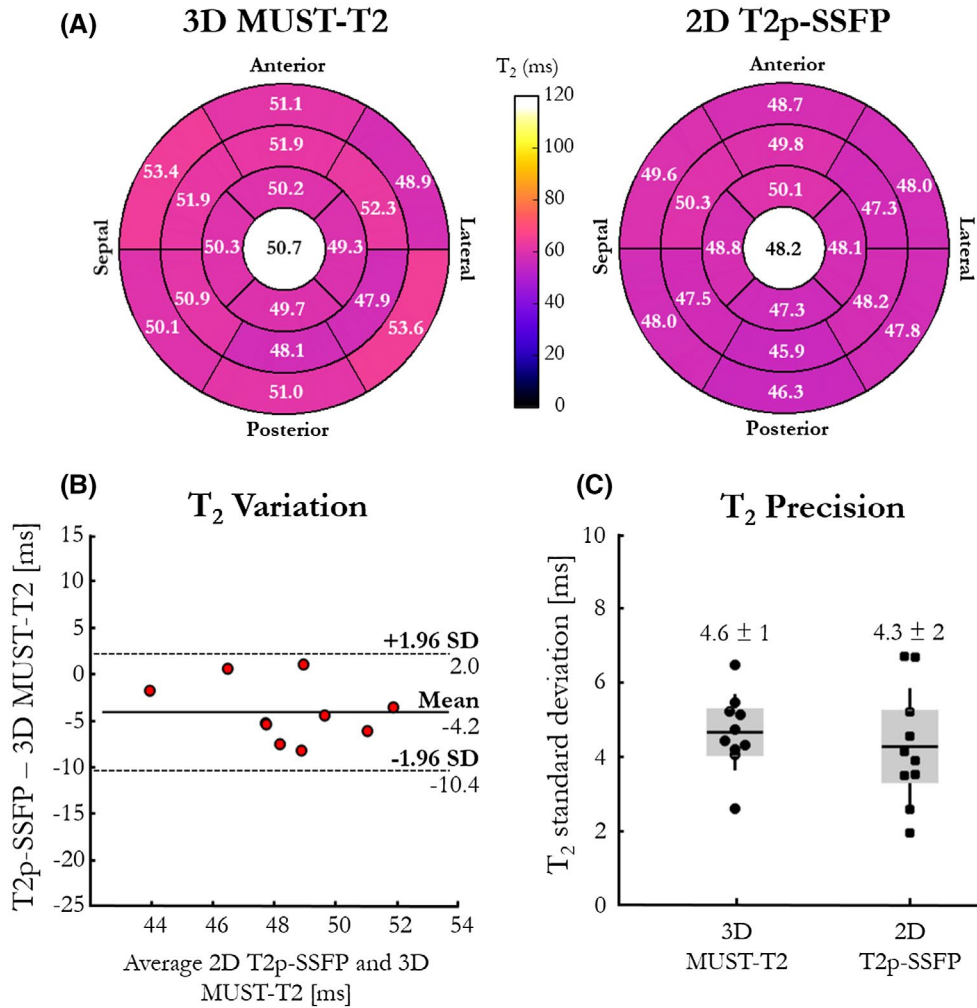


FIGURE 5 Accuracy and precision of the proposed 3D MUST-T₂ mapping sequence. A, The T₂ accuracy of the proposed 3D MUST-T₂ sequence versus conventional 2D T₂p-SSFP, as measured by the mean T₂ value, are shown in the left ventricular segmentation. The T₂ values are in good agreement with the literature (T₂ = 50 ± 4 ms³³). The averaged T₂ relaxation times over the whole myocardium are shown in the bull’s eye plots’ center. Accuracy (B) and precision (C) of T₂ relaxation times (ms) obtained in the myocardial septum with the proposed 3D MUST-T₂ and the conventional 2D T₂p-SSFP are shown for the 10 healthy subjects

Three-dimensional MUST-T₂ uses a saturation pulse to reset the magnetization immediately after the R-wave, as proposed by Ding et al,¹⁷ and therefore is mostly independent of heart-rate variations. Another advantage of using saturation pulses compared with other T₂ mapping techniques^{3,5,16,31} is that recovery periods between subsequent heartbeats are not needed, thus reducing the total acquisition time.

Further acceleration through undersampling is crucial to achieve high isotropic resolution in a clinically feasible scan time. In phantom experiments, we observed that acceleration factors of up to 5-fold led to accurate T₂ values (R² > 0.99) with respect to reference SE measurements. Besides the use of an efficient undersampling trajectory, the acquisition of low-resolution 2D iNAV’s at every heartbeat also permits a substantial reduction in scan time by allowing 100% respiratory scan efficiency (no data rejection) and predictable scan time,²⁴ as opposed to other respiratory-gated T₂ mapping techniques

based on diaphragmatic navigator-gated acquisition.¹⁷ Other free-breathing T₂ mapping techniques have been proposed to allow for 100% scan efficiency and predictable scan time. Van Heeswijk et al⁵ proposed a respiratory self-navigated 3D sequence to acquire isotropic 3D T₂ maps with resolution of 1.7 mm³ in a predictable scan time of about 18 minutes at 3 T, while Basha et al³² proposed a 2D multislice sequence with slice tracking. The significant scan-time reduction achieved with 3D MUST-T₂ was exploited to acquire in vivo isotropic whole-heart Cartesian T₂ maps in clinically feasible scan times (about 8 minutes), whereas a fully sampled acquisition would have required more than 35 minutes. The total imaging time for 3D MUST-T₂ was affected primarily by the subject’s heart rate and the number of slices needed to cover the whole heart in the anterior–posterior direction. For comparison, the conventional breath-hold 2D T₂p-SSFP sequence would have required between 5 and 7 minutes to cover the entire heart

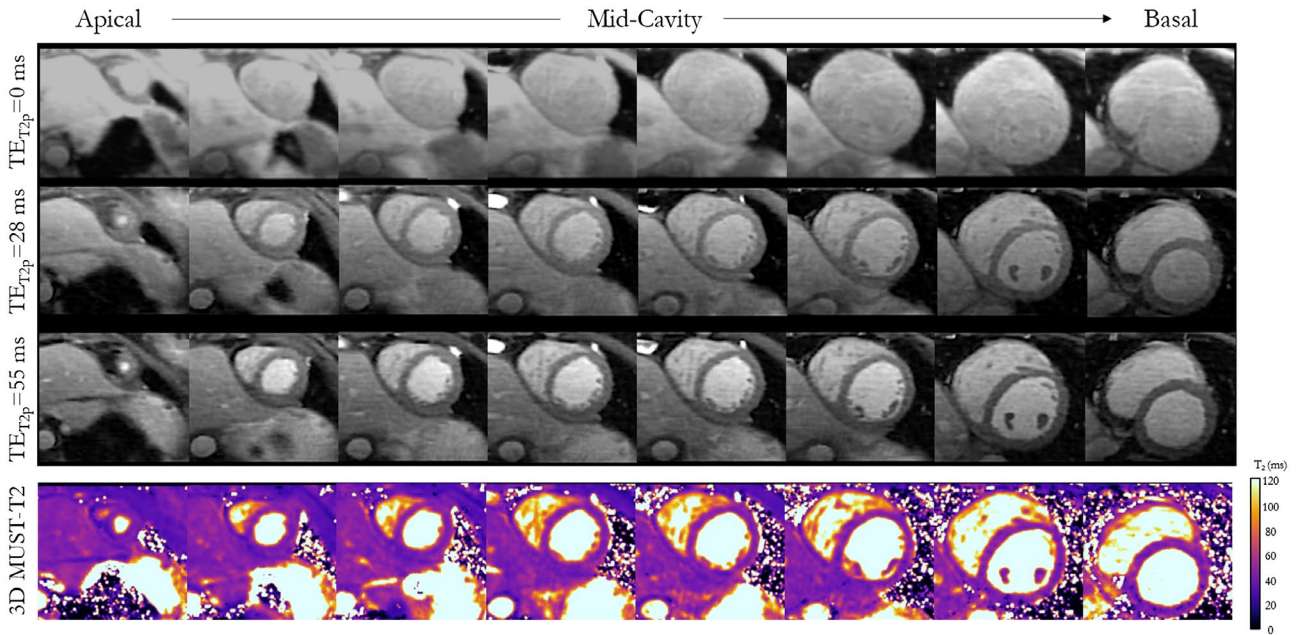


FIGURE 6 Three-dimensional visualization of the acquired T_2 -weighted images and the corresponding T_2 volume. Representative T_2 -weighted images for subject 2 (acquisition time: 10 minutes, heart rate = 38 bpm), and the corresponding T_2 maps obtained by the proposed 3D MUST- T_2 . Eight reformatted short-axis slices that cover the heart from apex to base are shown. Uniform distribution of T_2 values through the slices over the whole left ventricle can be observed. The color scale indicates T_2 values between 0 ms and 120 ms

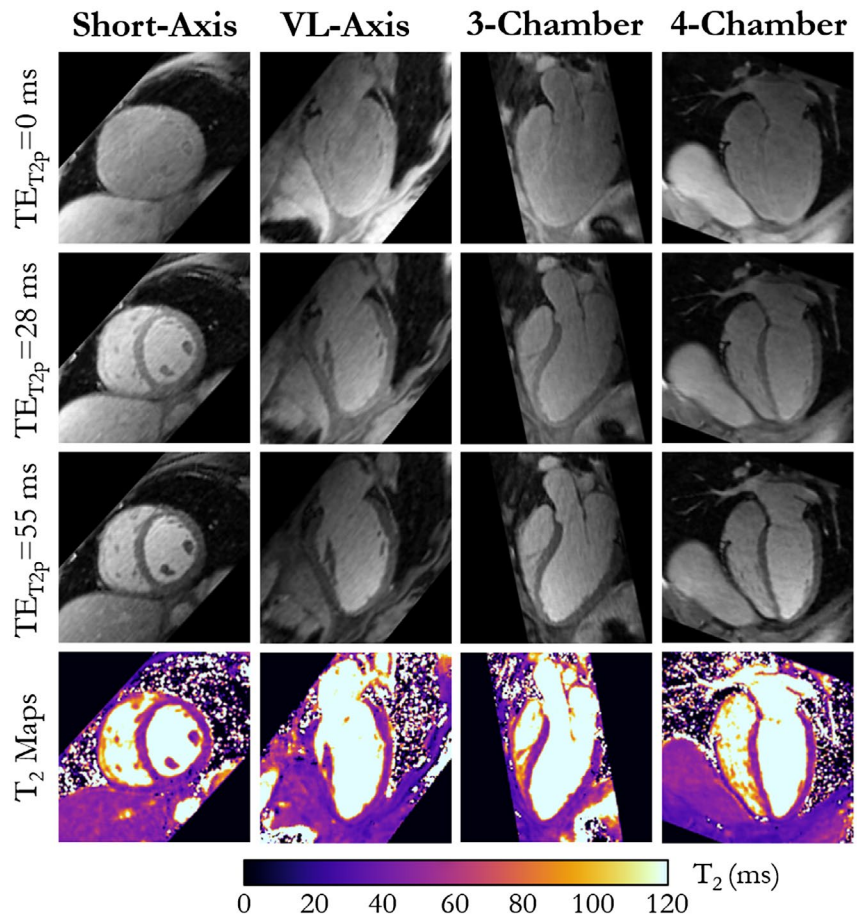


FIGURE 7 Representative T_2 -prepared images for subject 2 and the corresponding T_2 maps obtained with the proposed 3D MUST- T_2 sequence. Reformats in short-axis, vertical long-axis (VL), 3-chamber, and 4-chamber views are shown

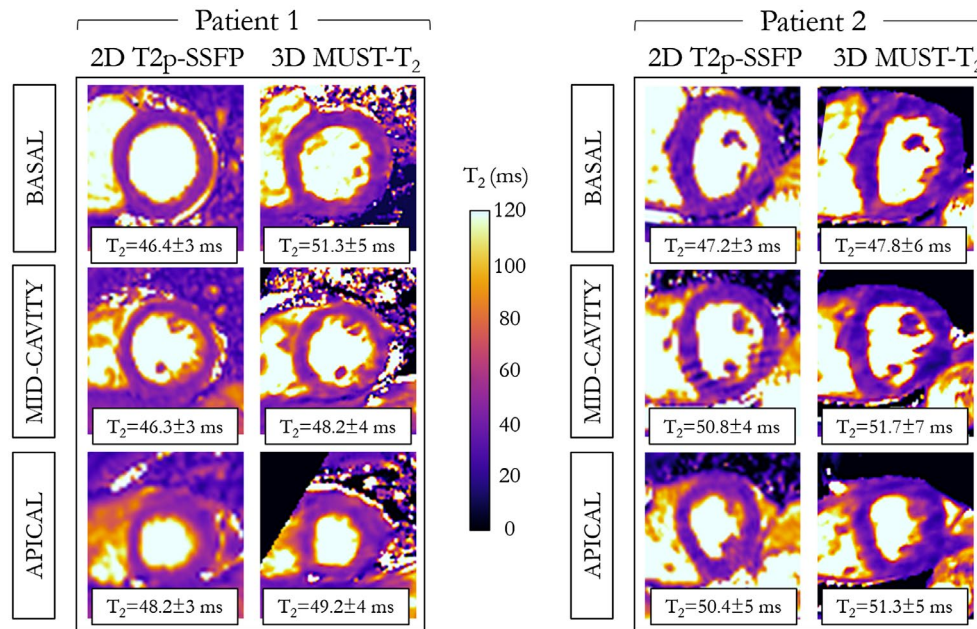


FIGURE 8 Short-axis T_2 maps at apical, midventricular, and basal level for 2 patients acquired with the proposed free-breathing 3D MUST- T_2 framework and the conventional breath-hold 2D T_2p -SSFP sequence. The septal T_2 relaxation times for each slice are reported as mean \pm SD

(assuming 7-second breathing commands, 10-second resting time between acquisitions, 10-second breath-hold, and assuming that 11 to 16 slices are needed to cover the heart). The proposed 3D T_2 mapping sequence can also be performed with lower anisotropic resolution (e.g., $2.0 \times 2.0 \times 6.0 \text{ mm}^3$ as achieved in Yang¹⁶), which will result in shorter scan times and inherently co-registered slices due to the 3D nature of the acquisition.

The acquisition of undersampled data comes, however, at the cost of significant loss of information that needs to be recovered. Multicontrast HD-PROST reconstruction takes advantage of the local, nonlocal, and contrast redundancies found in the T_2 -weighted images, to recover whole-heart T_2 maps with negligible remaining aliasing artifacts. The measurements of myocardial T_2 values by 3D MUST- T_2 in healthy subjects (average septal $T_2 = 50.8 \pm 3 \text{ ms}$) were in good agreement with in vivo values published in a previous study at 1.5 T with centric ordering ($T_2 = 50 \pm 4 \text{ ms}$ ³³). The T_2 overestimation with respect to the conventional breath-hold 2D T_2p -SSFP sequence was observed, with a bias of $4.2 \pm 6.2 \text{ ms}$. This overestimation was likely due to the choice of centric (3D MUST- T_2) versus linear (2D T_2p -SSFP) k-space ordering, as observed by Giri et al.³ Other confounding factors such as heart-rate variations³⁴ not present in the phantom study, or the use of fat saturation and adiabatic T_2 preparation pulses, could also explain this overestimation in vivo and will be explored further.

Although high acceleration factors were reached with the proposed 3D sequence, precision of T_2 values in vivo did not show significant deviations from the conventional 2D T_2p -SSFP acquisitions ($4.6 \pm 1 \text{ ms}$ versus $4.3 \pm 2 \text{ ms}$,

$P = .520$) and were similar to previously reported values at 3 T.^{5,17} This can be attributed to the good performance of HD-PROST reconstruction in concert with the variable-density trajectory with spiral profile order trajectory, which limits the propagation of noise in the T_2 -weighted images, noise being a severe side effect of saturation-based MR mapping techniques.^{16,35,36}

Dictionary-based matching was used in this study to accurately estimate myocardial T_2 values by pregenerating a dictionary representative of the proposed T_2 mapping sequence, and whose elements are composed of simulated signal evolution curves.²⁸ Our findings in phantom experiments showed that dictionary-based matching has the potential to accurately estimate myocardial T_2 values acquired with both 3D MUST- T_2 and conventional T_2p -balanced SSFP, whereas a T_2 bias was observed with conventional mono-exponential fitting for both methods (Supporting Information Figure S4). This can be partly explained by the fact that mono-exponential fitting does not accurately describe the acquisition parameters and the signal evolution during acquisition, such as balanced SSFP T_1/T_2 ratio of tissue, subject-specific heart rate, number of segments per heartbeat, and number of linear ramp-up pulses. Therefore, the use of dictionary-based matching could also improve conventional 2D T_2p -SSFP and potentially reduce the bias observed with linear phase encoding.

A limitation of the current framework is that only 2D translation respiratory motion correction was performed to ensure fast reconstruction times. It has been shown in previous reports that nonrigid motion registration can improve reproducibility and spatial variability of 2D T_2 mapping techniques.^{8,11} Although this issue was not shown to be significant

in the present experiments, it can be overcome by incorporating 3D nonrigid respiratory motion correction directly in the image reconstruction.³⁷⁻³⁹ Another alternative to deal with large motion between the T_2 -weighted images is to extend the proposed HD-PROST reconstruction to enable motion-resolved reconstruction by extending the searching neighborhood for patch selection to the spatial-temporal dimension.⁴⁰

In this study, middiastolic imaging was used to minimize cardiac motion and guarantee long saturation times. However, in subjects with highly variable heart rates or high heart rates, end-systolic imaging may be preferred. Future studies will investigate the effect of shorter saturation times on the accuracy and precision of saturation-based T_2 mapping; however, our phantom experiments demonstrate that accuracy is not affected for different heart rates between 50 and 100 bpm.

Moreover, incomplete saturation of fat signal can occur in some regions of the T_2 -weighted images, especially around the epicardial fat area. This effect can lead to fat-myocardium partial volume effect, apparent distortion, and loss of sharpness on the T_2 map and may alter the T_2 measurements. Further optimized fat suppression for each T_2 -weighted image will be investigated in the future to alleviate this difficulty.

Translational motion estimation and correction was performed inline in the scanner software, while HD-PROST reconstruction and dictionary matching were performed offline. The efficient multithreaded implementation of HD-PROST allowed for fast T_2 map reconstruction (in the order of 3 minutes). Further speedup to reach subminute runtime could be achieved by implementing the reconstruction on multiple GPUs and using coil compression strategies.⁴¹

It should be noted that 3D MUST- T_2 is based on a T_2 -prepared sequence that is used commonly in coronary MRA.⁴² The acceptable contrast provided by the last T_2 -weighted volume ($TE_{T_2\text{prep}} = 55$ ms, Figures 6 and 7) could also be exploited to visualize whole-heart cardiac and proximal coronary artery anatomy. Thus, 3D MUST- T_2 may be used for the simultaneous assessment of cardiac and coronary anatomy and myocardial T_2 relaxation times in a highly simplified and efficient single free-breathing acquisition. This additional gain could potentially benefit patients with acute non-ST-segment elevation myocardial infarction, where obstructive coronary artery disease and myocardial edema are often characteristic.¹³

The proposed free-breathing T_2 mapping framework could benefit many cardiovascular patients with severe shortness of breath and where imaging under breath-holding is often challenging. Preliminary insights into the potential of the proposed 3D MUST- T_2 mapping technique in a clinical setting was provided for 2 patients with suspected cardiovascular disease. Although no pathologies were observed in this proof-of-concept study, scanning patients often leads to new challenges (e.g., variable heart rate, irregular breathing pattern, poor compliance), resulting in degraded image quality.

Higher amplitude in respiratory motion of the heart, as provided by the 2D iNAVs, was observed in patients compared with healthy controls (Supporting Information Figure S9). The mean septal T_2 values measured on the 2 patients were comparable to that of the healthy subjects. Besides T_2 relaxation times conforming to the literature (Figure 8), the 3D whole-heart isotropic coverage of the proposed technique offers the opportunity to reformat the T_2 maps in any desired orientation, which can be particularly useful for the comprehensive assessment of pathological tissues with complex geometry.⁶

The proposed framework also shares similarities with the recent qBOOST- T_2 approach⁴³ that enables co-registered bright-blood and black-blood whole-heart imaging, together with T_2 quantification and coronary lumen visualization, through the use of an inversion pulse every 3 heartbeats. Although the latest technique may be preferred whenever coronary assessment or precontrast black-blood images are clinically required, a thorough comparison of the 2 approaches in large patient cohorts will need to be studied.

Finally, the proposed fast and efficient framework holds promise for wider cardiac applications, such as high-resolution motion-compensated 3D T_1 mapping and 3D joint T_1 - T_2 mapping,⁴⁴⁻⁴⁹ both of which will be investigated in future work.

5 | CONCLUSIONS

A novel approach was developed to enable free-breathing whole-heart 3D T_2 mapping with high isotropic spatial resolution (1.5 mm^3) in a clinically feasible scan time (< 8 minutes with 100% scan efficiency and predictable scan time). The proposed 3D MUST- T_2 framework achieved accurate T_2 quantification in phantom and in vivo with fast acquisition. Three-dimensional MUST T_2 mapping may have the potential to aid the management of many cardiomyopathies in which fast and efficient free-breathing acquisitions are key to patient comfort, whereas high isotropic resolution is crucial to accurately map tissue heterogeneity. Further studies to assess the clinical utility of 3D MUST- T_2 mapping in patients with myocardial inflammation are now warranted.

ACKNOWLEDGMENTS

Extended phase graph simulations were based on the algorithm described by Dr. Matthias Weigel,¹⁹ made available on the author's website. The authors acknowledge the financial support from EPSRC EP/P001009/, EP/P032311/1, EPSRC EP/P007619, Wellcome EPSRC Centre for Medical Engineering (NS/A000049/1), and the Department of Health through the National Institute for Health Research (NIHR) comprehensive Biomedical Research Centre award to Guy's

& St. Thomas' NHS Foundation Trust in partnership with King's College London and King's College Hospital NHS Foundation Trust. The views expressed are those of the authors and not necessarily those of the NHS, the NIHR, or the Department of Health.

CONFLICT OF INTEREST

Dr. Radhouene Neji is employed by Siemens Healthcare, Frimley, United Kingdom.

ORCID

Aurélien Bustin  <https://orcid.org/0000-0002-2845-8617>

Giorgia Milotta  <https://orcid.org/0000-0002-3403-3754>

René M. Botnar  <https://orcid.org/0000-0003-2811-2509>

Claudia Prieto  <https://orcid.org/0000-0003-4602-2523>

REFERENCES

- Guo H, Au W-Y, Cheung JS, et al. Myocardial T2 quantitation in patients with iron overload at 3 Tesla. *J Magn Reson Imaging*. 2009;30:394–400.
- He T, Gatehouse PD, Anderson LJ, et al. Development of a novel optimized breathhold technique for myocardial T2 measurement in thalassemia. *J Magn Reson Imaging*. 2006;24:580–585.
- Giri S, Chung Y-C, Merchant A, et al. T2 quantification for improved detection of myocardial edema. *J Cardiovasc Magn Reson*. 2009;11:1–13.
- Haberkorn SM, Spieker M, Jacoby C, Flögel U, Kelm M, Bönner F. State of the art in cardiovascular T2 mapping: on the way to a cardiac biomarker? *Curr Cardiovasc Imaging Rep*. 2018;11.
- Van Heeswijk RB, Piccini D, Feliciano H, Hullin R, Schwitler J, Stuber M. Self-navigated isotropic three-dimensional cardiac T2 mapping. *Magn Reson Med*. 2015;73:1549–1554.
- Ding H, Schar M, Zviman MM, Halperin HR, Beinart R, Herzka DA. High-resolution quantitative 3D T2 mapping allows quantification of changes in edema after myocardial infarction. *J Cardiovasc Magn Reson*. 2013;15:345–347.
- Van Heeswijk RB, Piccini D, Tozzi P, et al. Three-dimensional self-navigated T2 mapping for the detection of acute cellular rejection after orthotopic heart transplantation. *Transplant Direct*. 2017;3.
- Roujol S, Basha TA, Weingartner S, et al. Motion correction for free breathing quantitative myocardial T2 mapping: impact on reproducibility and spatial variability. *J Cardiovasc Magn Reson*. 2015;17:W5.
- Jin N, Jolly M-P, Raman SV, Simonetti OP. Free-breathing myocardial T2 mapping using GRE-EPI and automatic non-rigid motion correction. *J Cardiovasc Magn Reson*. 2015;17.
- Odille F, Escanyé JM, Atkinson D, Bonnemains L, Felblinger J. Nonrigid registration improves MRI T2 quantification in heart transplant patient follow-up. *J Magn Reson Imaging*. 2015;42:168–174.
- Giri S, Shah S, Xue H, et al. Myocardial T2 mapping with respiratory navigator and automatic nonrigid motion correction. *Magn Reson Med*. 2012;68:1570–1578.
- Rauhalammi S, Layland J, Carrick D, et al. T1 and T2 mapping have higher diagnostic accuracy for the ischaemic area-at-risk in NSTEMI patients compared with dark blood imaging. *Heart*. 2014;100.
- Tessa C, Del Meglio J, Lilli A, et al. T1 and T2 mapping in the identification of acute myocardial injury in patients with NSTEMI. *Radiol Med*. 2018;123:926–934.
- Puntmann VO, Isted A, Hinojar R, Foote L, Carr-White G, Nagel E. T1 and T2 mapping in recognition of early cardiac involvement in systemic sarcoidosis. *Radiology*. 2017;285:63–72.
- Van Heeswijk RB, Feliciano H, Bongard C, et al. Free-breathing 3T magnetic resonance T2-mapping of the heart. *JACC Cardiovasc Imaging*. 2012;5:1231–1239.
- Yang HJ, Sharif B, Pang J, et al. Free-breathing, motion-corrected, highly efficient whole heart T2 mapping at 3T with hybrid radial-cartesian trajectory. *Magn Reson Med*. 2016;75:126–136.
- Ding H, Fernandez-De-Manuel L, Schär M, et al. Three-dimensional whole-heart T2 mapping at 3T. *Magn Reson Med*. 2015;74:803–816.
- Bustin A, Cruz G, Jaubert O, Lopez K, Botnar RM, Prieto C. High-dimensionality undersampled patch-based reconstruction (HD-PROST) for accelerated multi-contrast magnetic resonance imaging. *Magn Reson Med*. 2019;81:3705–3719.
- Weigel M. Extended phase graphs: dephasing, RF pulses, and echoes—pure and simple. *J Magn Reson Imaging*. 2015;41:266–295.
- Nezafat R, Stuber M, Ouwerkerk R, Gharib AM, Desai MY, Pettigrew RI. B1-insensitive T2 preparation for improved coronary magnetic resonance angiography at 3T. *Magn Reson Med*. 2006;55:858–864.
- Prieto C, Doneva M, Usman M, et al. Highly efficient respiratory motion compensated free-breathing coronary MRA using golden-step Cartesian acquisition. *J Magn Reson Imaging*. 2015;41:738–746.
- Bustin A, Ginami G, Cruz G, et al. Five-minute whole-heart coronary MRA with sub-millimeter isotropic resolution, 100% respiratory scan efficiency, and 3D-PROST reconstruction. *Magn Reson Med*. 2019;81:102–115.
- Winkelmann S, Schaeffter T, Koehler T, Eggers H, Doessel O. An optimal radial profile order based on the golden ratio for time-resolved MRI. *IEEE Trans Med Imaging*. 2007;26:68–76.
- Henningson M, Koken P, Stehning C, Razavi R, Prieto C, Botnar RM. Whole-heart coronary MR angiography with 2D self-navigated image reconstruction. *Magn Reson Med*. 2012;67:437–445.
- Ginami G, Neji R, Phinikaridou A, Whitaker J, Botnar RM, Prieto C. Simultaneous bright- and black-blood whole-heart MRI for non-contrast enhanced coronary lumen and thrombus visualization. *Magn Reson Med*. 2018;79:1460–1472.
- Bustin A, Voilliot D, Menini A, et al. Isotropic reconstruction of MR images using 3D patch-based self-similarity learning. *IEEE Trans Med Imaging*. 2018;37:1932–1942.
- Hennig J, Weigel M, Scheffler K. Calculation of flip angles for echo trains with predefined amplitudes with the extended phase graph (EPG)-algorithm: principles and applications to hyperecho and TRAPS sequences. *Magn Reson Med*. 2004;51:68–80.
- Roccia E, Vidya Shankar R, Neji R, et al. Accelerated 3D T2 mapping with dictionary-based matching for prostate imaging. *Magn Reson Med*. 2019;81:1795–1805.
- Captur G, Gatehouse P, Keenan KE, et al. A medical device-grade T1 and ECV phantom for global T1 mapping quality

- assurance—the T1 mapping and ECV standardization in cardiovascular magnetic resonance (TIMES) program. *J Cardiovasc Magn Reson*. 2016;18:1–20.
30. Cerqueira MD, Weissman NJ, Dilsizian V, et al. Standardized myocardial segmentation and nomenclature for tomographic imaging of the heart: a statement for healthcare professionals from the cardiac imaging. *Circulation*. 2002;105.
 31. Darçot E, Yerly J, Colotti R, et al. Accelerated and high-resolution cardiac T2 mapping through peripheral k-space sharing. *Magn Reson Med*. 2019;81:220–233.
 32. Basha TA, Bellm S, Roujol S, Kato S, Nezafat R. Free-breathing slice-interleaved myocardial T2 mapping with slice-selective T2 magnetization preparation. *Magn Reson Med*. 2016;76:555–565.
 33. Blume U, Lockie T, Stehning C, et al. Interleaved T1 and T2 relaxation time mapping for cardiac applications. *J Magn Reson Imaging*. 2009;29:480–487.
 34. Granitz M, Motloch LJ, Granitz C, et al. Comparison of native myocardial T1 and T2 mapping at 1.5T and 3T in healthy volunteers: reference values and clinical implications. *Wien Klin Wochenschr*. 2019;131:143–155.
 35. Nordio G, Bustin A, Henningsson M, et al. 3D SASHA myocardial T1 mapping with high accuracy and improved precision. *Magn Reson Mater Phys Biol Med*. 2019;32:281–289.
 36. Bustin A, Ferry P, Codreanu A, et al. Impact of denoising on precision and accuracy of saturation-recovery-based myocardial T1 mapping. *J Magn Reson Imaging*. 2017;46:1377–1388.
 37. Odille F, Menini A, Escanye J-M, et al. Joint reconstruction of multiple images and motion in MRI: application to free-breathing myocardial T2 quantification. *IEEE Trans Med Imaging*. 2016;35:197–207.
 38. Batchelor PG, Atkinson D, Irrazaval P, Hill D, Hajnal J, Larkman D. Matrix description of general motion correction applied to multishot images. *Magn Reson Med*. 2005;54:1273–1280.
 39. Cruz G, Atkinson D, Henningsson M, Botnar RM, Prieto C. Highly efficient nonrigid motion-corrected 3D whole-heart coronary vessel wall imaging. *Magn Reson Med*. 2017;77:1894–1908.
 40. Kuestner T, Bustin A, Cruz G, et al. 3D Cartesian free-running cardiac and respiratory resolved whole-heart MRI. In: Proceedings of the 27th Annual Meeting of ISMRM, Montreal, Canada, 2019. p 2192.
 41. Zhang T, Pauly JM, Vasawala SS, Lustig M. Coil compression for accelerated imaging with Cartesian sampling. *Magn Reson Med*. 2013;69:571–582.
 42. Botnar RM, Stuber M, Danias PG, Kissinger KV, Manning WJ. Improved coronary artery definition with T2-weighted, free-breathing, three-dimensional coronary MRA. *Circulation*. 1999;99:3139–3148.
 43. Milotta G, Ginami G, Bustin A, Neji R, Prieto C, Botnar RM. 3D whole-heart free-breathing BOOST-T2 mapping. In: Proceedings of the 27th Annual Meeting of ISMRM, Montreal, Canada, 2019. p 2002.
 44. Akçakaya M, Weingärtner S, Basha TA, Roujol S, Bellm S, Nezafat R. Joint myocardial T1 and T2 mapping using a combination of saturation recovery and T2-preparation. *Magn Reson Med*. 2016;76:888–896.
 45. Kvernby S, Warntjes M, Haraldsson H, Carlhäll CJ, Engvall J, Ebberts T. Simultaneous three-dimensional myocardial T1 and T2 mapping in one breath hold with 3D-QALAS. *J Cardiovasc Magn Reson*. 2014;16:102.
 46. Xanthis CG, Bidhult S, Greiser A, et al. Simulation-based quantification of native T1 and T2 of the myocardium using a modified MOLLI scheme and the importance of magnetization transfer. *Magn Reson Imaging*. 2018;48:96–106.
 47. Guo R, Chen Z, Herzka DA, Luo J, Ding H. A three-dimensional free-breathing sequence for simultaneous myocardial T1 and T2 mapping. *Magn Reson Med*. 2018;81:1031–1043.
 48. Santini F, Kawel-Boehm N, Greiser A, Bremerich J, Bieri O. Simultaneous T1 and T2 quantification of the myocardium using cardiac balanced-SSFP inversion recovery with interleaved sampling acquisition (CABIRIA). *Magn Reson Med*. 2015;74:365–371.
 49. Milotta G, Ginami G, Bustin A, Neji R, Prieto C, Botnar RM. 3D whole-heart high-resolution motion compensated joint T1/T2 mapping. In: Proceedings of the 27th Annual Meeting of ISMRM, Montreal, Canada, 2019. p 2003.

SUPPORTING INFORMATION

Additional supporting information may be found online in the Supporting Information section at the end of the article.

FIGURE S1 A 3D Cartesian variable-density trajectory was used to allow for fast acquisition of multiple T_2 -weighted images. The Cartesian trajectory with spiral order samples the k_y - k_z phase-encoding plane following approximate spiral interleaves on the Cartesian grid with variable density along each spiral arm. In this sketch, the 2 first acquired spirals are shown for each contrast (each spiral containing 20 segments). A golden angle rotation between successive spirals and successive contrasts is applied to introduce incoherently distributed aliasing artifacts along the contrast dimension, and noise-like artifacts in the spatial dimension

FIGURE S2 Flowchart of the optimization 2 of the proposed HD-PROST. Denoising of multiple T_2 -weighted images is performed using a 3D block matching, which groups and unfolds similar 3D patches in the noisy multicontrast images to form a low-rank 2D matrix. A third-order tensor is formed by stacking the T_2 contrast dimension on the third dimension. The high-order tensor of size N (number of pixels in each patch) $\times K$ (number of similar patches within a neighborhood) $\times L$ (number of T_2 contrasts) admits a low multilinear rank approximation and can be compressed through high-order tensor decomposition by truncating the multilinear singular vectors that correspond to small multilinear singular values. The outputs of this step are the denoised multicontrast images that are then used in the joint regularized reconstruction step (optimization 1) as prior knowledge. Reconstruction parameters used in this study are shown (bottom row). We refer the reader to Bustin et al¹⁸ for more information on these parameters. Reconstruction parameter details: L , number of contrasts; K , number of similar patches; N , patch size (in pixels); λ_p , threshold value

FIGURE S3 Simulations of the proposed T_2 mapping sequence were performed using the EPG formalism to assess the effect of T_1 in the EPG-based dictionary on the matched T_2 value. Signal evolutions for different T_1 (from 850 to 1200 with a step size of 50 ms) and T_2 (from 42 to 82 with a step size of 8 ms) were generated and matched to a dictionary simulated with fixed T_1 (1100 ms) and varying T_2 s (similar to the one used in the phantom experiment). A, Matched T_2 is plotted as a function of T_1 . B, The signal evolutions corresponding to short ($T_1/T_2 = 800/52$ ms), medium ($T_1/T_2 = 1100/52$ ms), and long ($T_1/T_2 = 1300/52$ ms) T_1 myocardium were generated for the proposed sequence through EPG simulation. The obtained signal evolutions did not appear to differ, suggesting that the proposed 3D MUST- T_2 map sequence with dictionary-based matching is independent of the T_1 used in the EPG-based dictionary (matched T_2 s were the same for the 3 generated signals and equal to 52 ms). Therefore, for the phantom and in vivo experiments, we kept the T_1 constant at 1100 ms

FIGURE S4 Conventional mono-exponential fitting and dictionary-based matching for T_2 T_2 p-SSFP T_2 mapping in comparison to the proposed 3D MUST- T_2 sequence for the phantom study. The proposed 3D acquisition with mono-exponential fitting is also included for comparison purposes. Accurate phantom T_2 values, in agreement with reference spin echo, were obtained with the proposed 3D MUST- T_2 sequence with dictionary-based matching; however, bias is observed with the proposed acquisition when mono-exponential fitting is used. Bias is also observed with the conventional (linear phase encoding) 2D T_2 p-SSFP mapping with mono-exponential fitting; however, this bias is significantly reduced when dictionary-based matching is used

FIGURE S5 Spatial T_2 uniformity over the slice direction is assessed for the phantom study for 3 vials (corresponding to short, medium, and long T_1 myocardium). The solid line is the average difference between gold-standard spin echo and the proposed 3D MUST- T_2 mapping sequence, and the dashed lines represent the mean ± 2 SDs between the 2 techniques. Good T_2 uniformity can be observed with the proposed technique. The mean difference in T_2 for the vial corresponding to short T_1 myocardium was -0.6 ms [$\pm 95\%$ confidence interval [CI] = $-2.1/0.89$ ms), -0.6 ms [$\pm 95\%$ CI = $-3.7/2.5$ ms) for the medium T_1 myocardium,

and -1.4 ms [$\pm 95\%$ CI = $-4.9/2.0$ ms) for the long T_1 myocardium

FIGURE S6 The T_2 maps obtained using the proposed free-breathing 3D MUST- T_2 mapping sequence and the conventional breath-held 2D T_2 p-SSFP sequence are shown for 3 additional healthy subjects. The 3D MUST- T_2 slices were reformatted to short axis to match the 2D T_2 map acquisitions. Representative 16 American Heart Association segments are shown to illustrate how much spatial information was considered for T_2 calculation. Acquisition times are expressed as minutes:seconds

FIGURE S7 Axial view of T_2 maps acquired using the proposed 3D T_2 mapping sequence on 3 healthy subjects. Number of slices was adjusted per subject to cover the left ventricle in the anterior–posterior direction

FIGURE S8 Impact of iNAV-based beat-to-beat translation motion correction on 3D MUST- T_2 map is shown for 2 healthy subjects. A, Reconstructed T_2 -weighted images ($TE_{T_2\text{prep}} = 55$ ms) are shown before and after motion correction with the corresponding T_2 maps. Better visualization of the myocardium can be observed after motion correction with clear delineation of cardiac structures and myocardial walls. Note the blurring observed on the non-motion-corrected T_2 maps. B, Plots showing the intensity profiles taken on the T_2 -weighted images through the heart–liver interface

FIGURE S9 A, Foot–head respiratory displacements of the heart obtained from the 2D image navigators at each heart-beat are shown for 2 representative healthy subjects (left) and 2 patients (right). The end-expiration position is used as reference for translational motion estimation. Although regular breathing patterns can be observed on the healthy subjects, more irregular breathing patterns with strong motion amplitudes are observed on patients 1 and 2. B, Average R-R intervals are shown for each healthy subject and patient. Patient 1 presented with irregular cardiac rhythm (R-R = 838 ± 211 ms)

How to cite this article: Bustin A, Milotta G, Ismail TF, Neji R, Botnar RM, Prieto C. Accelerated free-breathing whole-heart 3D T_2 mapping with high isotropic resolution. *Magn Reson Med*. 2020;83:988–1002. <https://doi.org/10.1002/mrm.27989>